applied sciences

MDPI

Article

Semi-Quantitative Analysis of Major Elements and Minerals: Clues from a Late Pleistocene Core from Campos Basin

Guilherme A. Pedrão *, Karen B. Costa, Felipe A. L. Toledo, Mariana O. Tomazella and Luigi Jovane

Instituto Oceanográfico, Universidade de São Paulo, Praça do Oceanográfico, 191 Cidade Universitária, 05508-120 São Paulo, Brazil; karen.costa@usp.br (K.B.C.); ftoledo@usp.br (F.A.L.T.); mariana.tomazella@usp.br (M.O.T.); jovane@usp.br (L.J.)

* Correspondence: guilherme.pedrao@usp.br

Abstract: Element and mineral associations are fundamental parameters for palaeoceanographical reconstructions but laboratory methodologies are expensive, time-consuming and need a lot of material. Here, we investigate the quality and reliability of XRF measurements of major elements (Fe, Ti and Ca) using BTX II Benchtop, by comparing them with previous ICP-OES elemental analysis for a set of Late Pleistocene marine sediments from Campos Basin. Although the numerical values of the logarithmic form of the elementary ratios were different, the lnTi/Ca and lnFe/Ca ratios measured by both techniques (XRF and ICP-OES) presented similar downcore results. To correct the XRF intensity data, a linear regression model was calculated and, based on the linear equation generated, the logarithmic values of the elementary XRF ratios were corrected. After the correction, One-Sample *t*-test and Bland–Altman plot show that both techniques obtained similar results. In addition, a brief paleoceanographic interpretation, during the MIS 5 and MIS 4 periods, was conducted by comparing mineralogical and elementary analysis aiming to reconstruct the variations of the terrigenous input to the studied area. As a conclusion, the results from XRF measurements (BTX II) presented to confirm the viability of such a technique, showing that analysis using BTX II is a reliable, cheap, rapid and non-destructive option for obtaining elementary ratios and mineralogical downcore results at high resolution, allowing stratigraphic and paleoceanographic interpretations.

Keywords: X-ray fluorescence; ICP-OES; elementary ratios; Fe/Ca; Ti/Ca; Campos Basin (Brazil); MIS 4; MIS 5

Citation: Pedrão, G.A.; Costa, K.B.; Toledo, F.A.L.; Tomazella, M.O.; Jovane, L. Semi-Quantitative Analysis of Major Elements and Minerals: Clues from a Late Pleistocene Core from Campos Basin. *Appl. Sci.* **2021**, *11*, 6206. https://doi.org/10.3390/app11136206

Academic Editor: Mónica Calero de Hoces

Received: 18 May 2021
Accepted: 27 June 2021
Published: 5 July 2021

1. Introduction

The investigations of mineral and elemental composition of bulk sediments are extremely important in the field of marine geology because they are directly related to paleoclimate, source-to-sink processes, marine primary productivity and post-depositional changes. The main expression of those processes is the glacial–interglacial alternations along the Quaternary period, which produce contrasting depositional regimes on the continental shelf and on the slope on the Brazilian Margin [1–4]. There are still uncertainties on how those processes express in terms of mineralogical and elemental abundances on slope environment in a tropical climate. This lack is related to the fact that minerals and elements are time-consuming, expensive, and need several grams of material that is completely destroyed during the measurements.

The study of elemental ratios in marine sediment cores using X-ray fluorescence (XRF) analysis is a valuable technique, which is cheap, rapid, and non-destructive, and so has enormous potentials for stratigraphic and paleoceanographic studies. XRF defines the concentrations of chemical elements and, consequently, minerals in the sample, or directly in the core, obtaining several key information from the past climate, oceanography and atmosphere (e.g., [1,5–7]).

The principle of XRF analysis is based on the excitation of electrons by incident X-radiation. The fluorescence energy is detected by a characteristic wavelength spectrum of

specific elements, which permits the estimation of their relative abundances [8]. Although the XRF is the most common technique to analyze the elemental concentrations of the bulk marine sediments [9], some destructive techniques can be applied, using devices such as Inductively Coupled Plasma-Optical Emission Spectrometry (ICP-OES).

ICP is an atomic emission technique, which measures the energy of an atom that returns to the ground state by emitting a photon, passing from an excited state to a lower energy state. The number of photons emitted is proportional to the number of atoms of the element present [10]. Therefore, it is possible to analyze and identify the elements in the sample, by separating the emitted light into its spectral components, using a high-performance spectrometer. The ICP-OES reaches a precision and accuracy of 5% for major element ratios, as determined by analyzing certified standards of contaminated soils (SS-1 and SS-2 EnviroMAT), which gives an excellent validation reference to our study.

The Olympus BTX II benchtop equipment combines XRF with X-ray diffraction (XRD) techniques on stratigraphical samples or discrete specimens directly collected from cores. This equipment performs one measurement in 10–20 min technique and needs a very small amount of dry material (3 mg) with no particular preparation, which can be used again for other measurements because it is non-destructive. This analytical technique reveals detailed structural information about the crystallography of materials and can be also applied in several paleoceanographic/climatology studies [11,12]. This XRD/XRF device is ideal to perform a general analysis of bulk material in the field and in the laboratory, by combining the techniques, allowing a better and more complete characterization of any given crystalline sample, that can be used in paleoceanographic or paleoclimatic studies [13–15] as well as in extraterrestrial missions [16,17].

Here, we investigate the efficiency of XRF measurements of major elements (Fe, Ti and Ca) using BTX II Benchtop, by comparing them with previous ICP-OES elemental analysis for a set of marine sediments recovered from piston core GL-451 (21°09.8′ S; 39°57.2′ W), located in the Brazilian Continental Margin [18], and compare the results obtained from this technique with data from XRD measurements to identified different patterns of terrigenous input to the studied area.

2. Materials and Methods

2.1. Marine Sediment Core

The performance of the BTX II Benchtop XRF (Olympus, Woburn, USA) was evaluated by investigation of 20 samples from the sediment piston core GL-451, which was retrieved from the continental slope of the Campos Basin (Rio de Janeiro, Brazil), at a 1503 m water depth (Figure 1). These samples were selected from Costa et al. [18] that cover the greatest amplitudes of environmental variability observed along the period studied, thus including the main gradients of environmental variability, enabling the discussion of both methodological validation and paleoclimatic application.

The continental supply in this region is controlled mainly by variations in precipitation, which influences directly the discharge of the two main rivers responsible for transport the continental input into the slope region: the Paraíba do Sul and the Doce River [18,19].

The chronology of the GL-451 core was previously established by Costa et al. [18], based on the variation of oxygen stable isotopes measured in benthic foraminifera. The lithology of the core was based on its carbonate content, being separated in carbonate-rich mud (30–60%) and carbonate-poor mud (20–10%) (Figure 2, see Costa et al. [18] for more details). For the present study, the samples ranging from 600 cm to 1200 cm were selected, which allows study the period between 59 kyrs BP and 100 kyrs BP, to investigate the efficiency of XRF measurements of major elements and compare these results with the mineralogy changes occurring along the marine isotope stage (MIS) transition from MIS 5 to MIS 4.

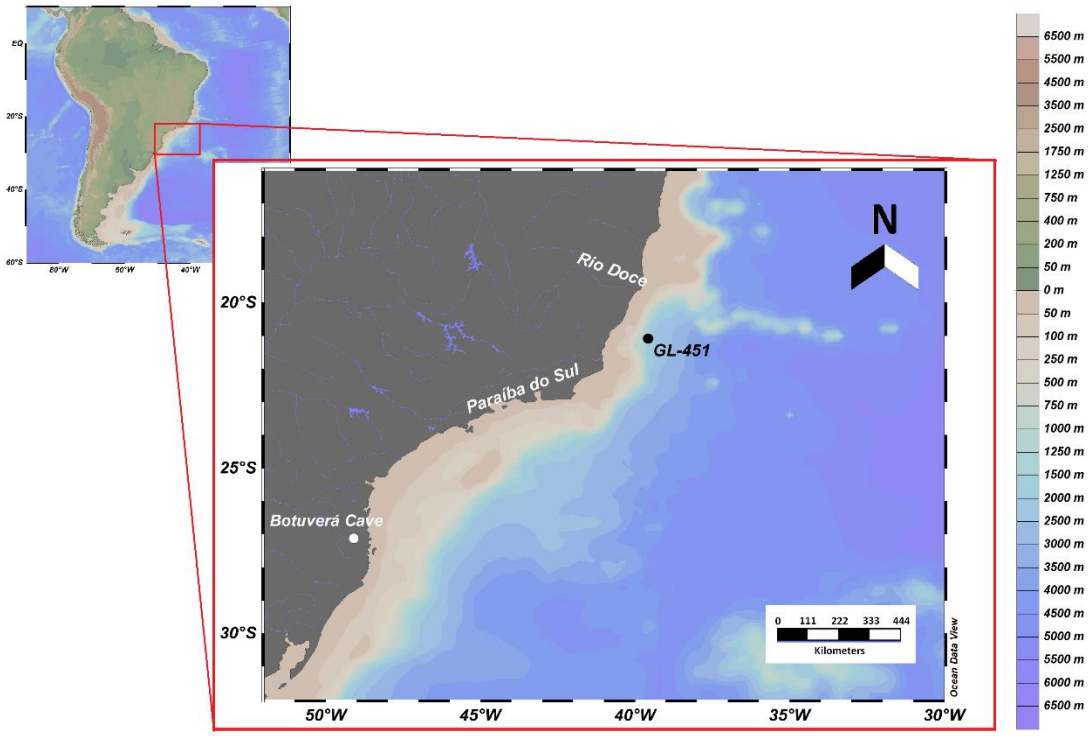

Figure 1. Region studied with the location of the core GL-451, Botuverá cave and the main rivers that contributes to the terrigenous supply, using the software Ocean Data View [20]. Modified from Wang et al. [21], based on Costa et al. [18].

2.2. XRD and XRF Analysis

Costa et al. [18], at the Laboratory of Marine Inorganic Chemistry (LAQIMAR—IOUSP), originally analyzed the same samples, using a Varian Inductively Coupled Plasma-Optical Emission Spectrometry, model VISTA-MPX. Therefore, the samples were re-analyzed to determine if BTX II Benchtop XRF measurements ensure precision and consistent measurements. The selected samples were prepared as described below.

The first step of sample preparation was the weighing of the humid bulk sample. After this, the samples were heat-dried at less than 60 °C in a laboratory stove and then weighed again to obtain the dry weight. The next step was the wet sieving in a 63 μm mesh. The fraction >63 μm was weighted and stored for future foraminiferal analysis. Approximately 1 cm3 of sediment (<63 μm fraction) per sample was hand-ground in a jade mortar to be used in the XRF analysis. This size fraction was selected due to the smaller interference in the intensity values measured by the Olympus BTX II Benchtop XRD/XRF device (Olympus, Woburn, MA, USA).

The measurements were performed in the Centro Oceanográfico de Registros Estratigráficos (CORE) at the Instituto Oceanográfico from Universidade de São Paulo. This equipment utilizes a cobalt source to perform XRD/XRF measurements that generate noise in the iron trace reading, causing overestimation. To eliminate noise, a 99% calcium carbonate (Merck, Darmstadt, Germany) sample, with small amounts of iron (concentration < 0.001%), was used and subtracted.

It is also important to point out that XRF is a semi-quantitative analysis able to support variations in the core depths. Since each element has its peak of intensity in a different quantity of incident energy. It is possible to compare the data of every sample, relating how was the variation of intensity in any sample at every depth of the core.

To determine the optimal number of expositions, diffractograms were obtained with different exposure times, and the best time/resolution was found at 100 exposures. The average energies utilized for peaks (Ka) intensity measurement were: 3.70 keV for Calcium, 4.49 keV for Titanium, and 6.43 keV for Iron.

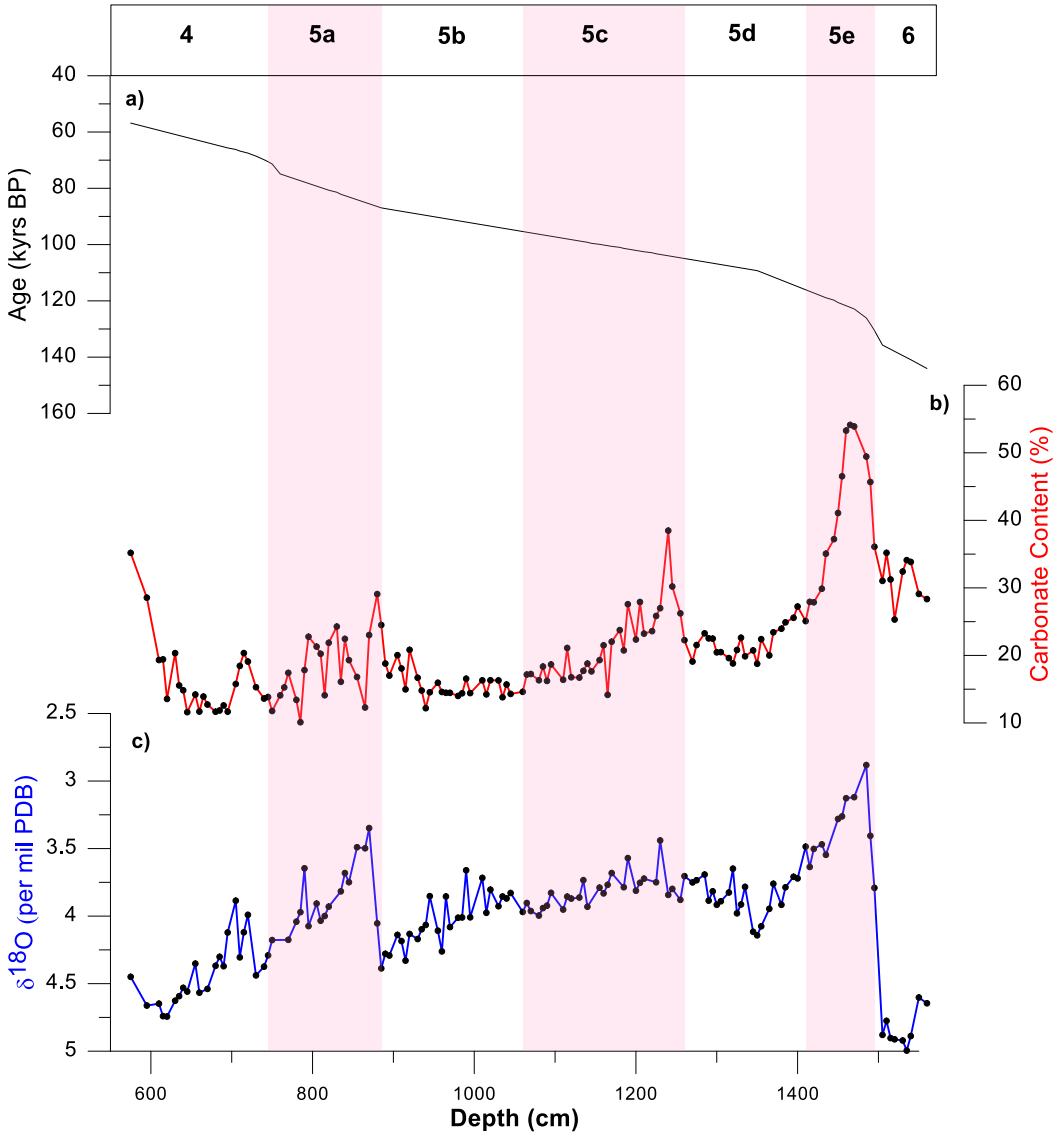

Figure 2. (**a**) Depth vs. age model of the core GL-451. (**b**) Carbonate content (%). (**c**) Benthic foraminifera (*Cibicidoides wuellerstorfi*) $\delta^{18}O$ record. Modified from Costa et al. [18].

To analyze the elemental ratios, the intensity data were transformed and presented in the logarithmic form of elementary rates. According to Weltje and Tjallingii [8], unlike the analyses that use the elements separately, elementary ratios are not subjected to dilution effects, avoiding the lack of symmetry exhibited by ratios.

The BTX II applies at the same time the XRD and XRF techniques, therefore, additionally to the elementary analyses, mineralogical data were also obtained. After the measures, semi-quantitative analysis was conducted with the High Score plus version 3.0 software [22], with the goal to identify the minerals present in the samples and then observe the variations of the main mineral constituents along the different studied periods. The data were then presented in percentages of the main mineral constituents.

2.3. Data Analysis

The obtained data from the XRF and ICP-OES techniques were submitted to Shapiro-Wilk's test, in order to test the Gaussian distribution. After the normality test, the variables were conducted to a Pearson correlation analysis to determine the degree of association between the two different techniques.

Attempting to better calibrate the XRF intensity, we use the ICP-OES data as a sample with known elementary ratios and calculated a linear regression model. Then, to compare the dissimilarity of the results obtained after the calibration, a One-Sample *t*-test, were applied with a given mean = 0, on the differences between the logarithmic values obtained in each technique. In addition, to make sure that the results are robust, a Bland–Altman plot (B-A plot), which is a widely used technique to compare the difference between two different methods [23–25], was also realized to compare the differences of the techniques.

The PAST™ software version 3.22 [26] was used to do the statistical analysis, besides only the B-A plot that was calculated separately.

3. Results

3.1. XRF Technique and Elementary Ratios

The lnTi/Ca varied between 1 and −1, while the lnFe/Ca −0.4 and −2.8. The elementary ratios showed mirror distributions, with higher values during the MIS 5b, a rapid decrease in the MIS 5a and maximum values along the MIS 4.

For comparison purposes, the selected samples were from the same GL451 depths for ICP-OES and XRF analysis of the same elements. The lnTi/Ca and lnFe/Ca ratios measured by both approaches (XRF and ICP-OES), presented similar downcore results (Figure 3), although the numerical values of the logarithmic form of the elementary ratios were different due to lack of equipment calibration (Table 1).

Table 1. Summary statistics for the samples (n = 20). The values are for the logarithmic form of the elementary ratios.

	ln (Ti/Ca)		**ln Fe/Ca**	
	XRF	**ICP-OES**	**XRF**	**ICP-OES**
Min	−2.087	−2.733	−0.341	−0.911
Max	−0.481	−1.130	0.837	0.376
Mean	−0.993	−1.683	0.389	−0.146
Std. Error	0.090	0.096	0.077	0.092
Variance	0.162	0.183	0.118	0.171
Stand. dev	0.402	0.428	0.344	0.413
Shapiro–Wilk W	0.924	0.906	0.913	0.924
p (normal)	0.117	0.053	0.072	0.118

All the variables presented p-values over 0.05 in the Shapiro–Wilk's test and therefore have a normal distribution (Table 1), allowing a Pearson correlation analysis. The correlations showed a significance value smaller than 0.01, with positive correlations observed for both lnTi/Ca (r = 0.935) and lnFe/Ca (r = 0.869).

Both linear regression models calculated demonstrated high r^2 values, 0.875 for lnTi/Ca and 0.755 for lnFe/Ca (Figure 4). The One-Sample T test presented p values higher than 0.05 for both elementary ratios, lnTi/Ca (p = 0.983) and lnFe/Ca (p = 0.869).

The B-A, as well as the *t*-test, also show that the mean of the differences is virtually zero, with the bias (mean of the differences between techniques) being 0.001 for lnTi/Ca and 0.002 for lnFe/Ca. All of the points were within the 95% confidence interval, with only one exception in the lnTi/Ca analysis (Figure 5).

3.2. Mineralogical Composition of the Sediments

The XRD analyses showed that the major minerals present in the core samples are Quartz and Calcite, generally being more than 80% of the mineral content in the samples (Figure 6a,b). The mineralogical analysis also founded Kaolinite and silica in the samples, however in the smaller presence and in fewer samples.

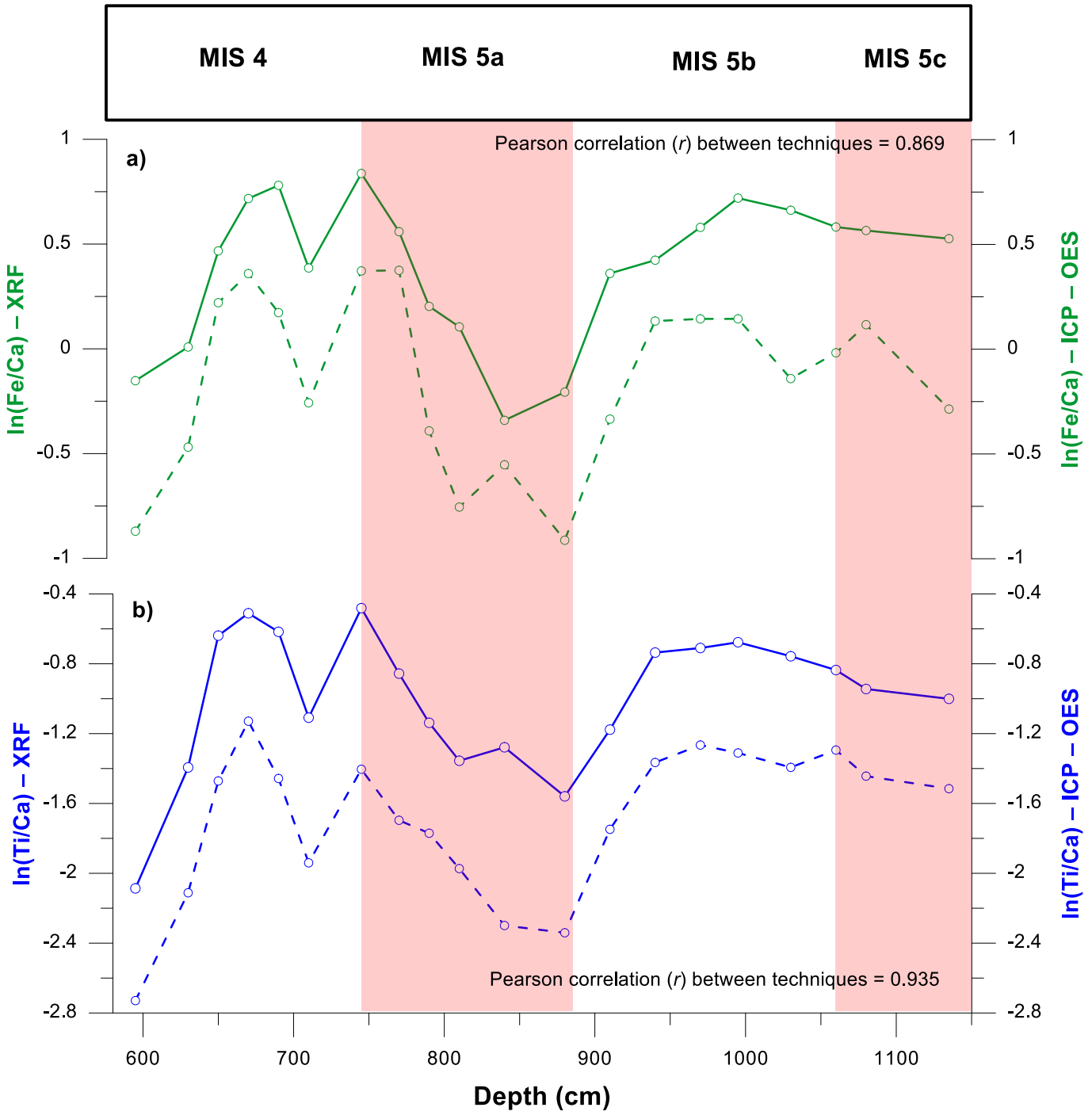

Figure 3. Comparison between the XRF (solid line) and ICP-OES (dashed line) techniques for the (**a**) ln(Fe/Ca) and (**b**) ln(Ti/Ca) ratios along the depths of the core. The values of the ratios obtained by XRF are on the left, while ICP-OES on the right. Pearson correlation estimated between the techniques is shown in each a and b Figures.

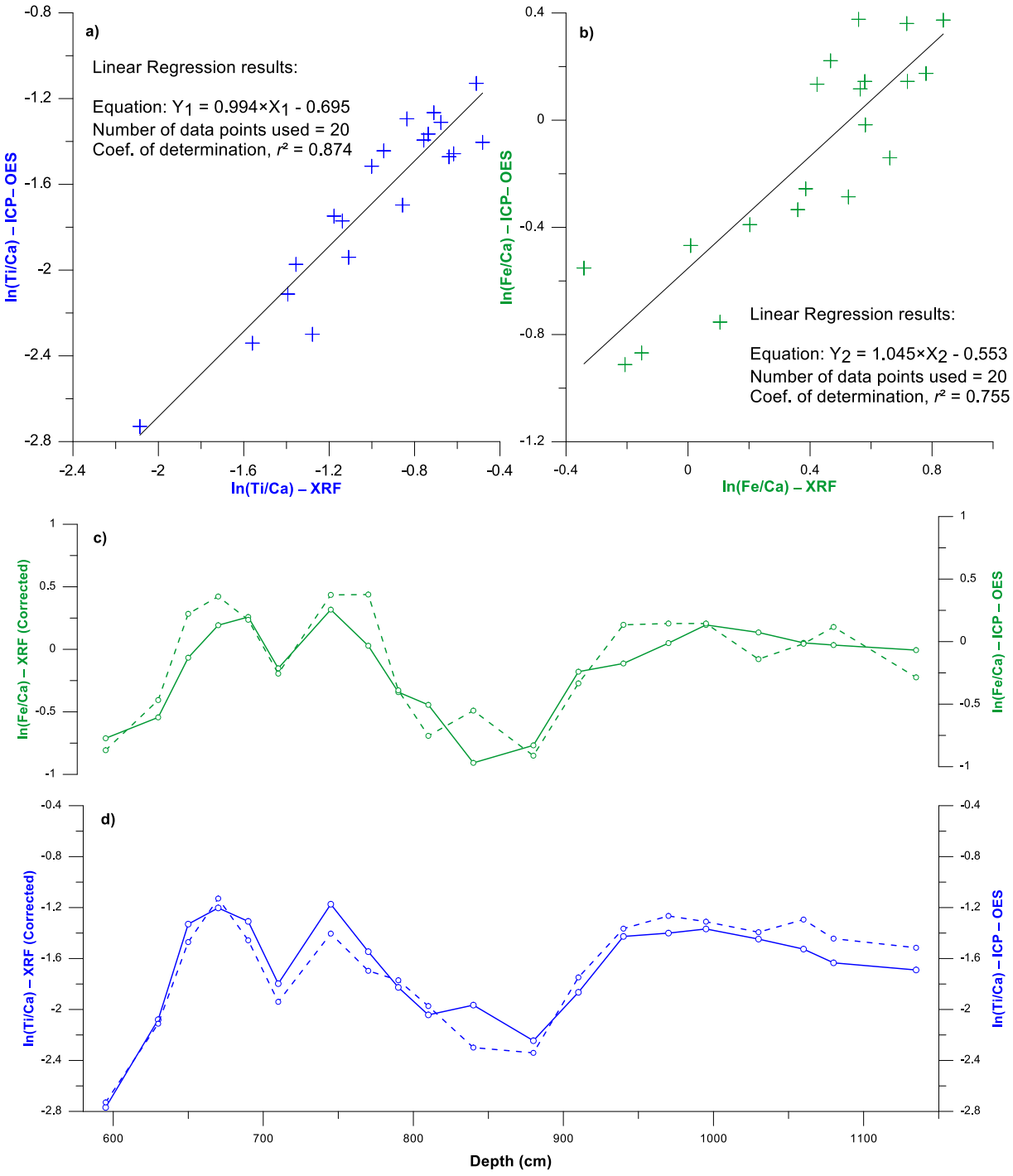

Figure 4. Results of the linear regression models calculated for (**a**) ln (Ti/Ca) and (**b**) ln (Fe/Ca). Comparison between the XRF corrected data (solid line) and ICP-OES (dashed line) techniques for the (**c**) ln(Fe/Ca) and (**d**) ln(Ti/Ca) ratios along the depths of the core. After the correction using the linear regression the techniques exhibit very similar results showing that the BTX equipment is able to perform well the analysis.

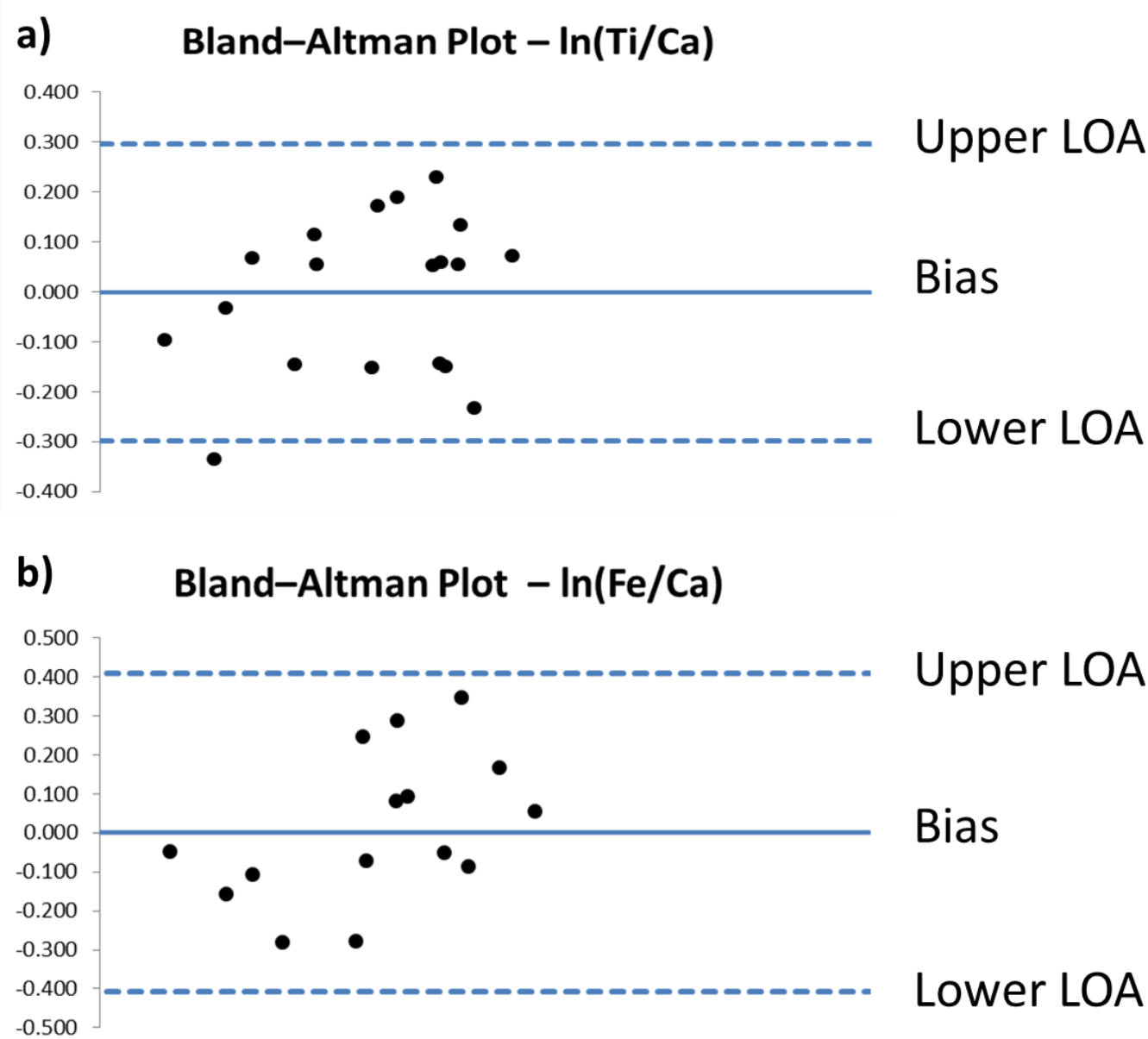

Figure 5. Bland–Altman plot for the (**a**) ln (Ti/Ca) and (**b**) ln (Fe/Ca) data. The straight line is the bias (mean of the differences). The dashed lines are for the limits of agreement calculated based on two standard deviations. The mean difference of the techniques for both ratios was close to zero and only one value for ln (Ti/Ca) was out of the LOA, highlighting the similar results between techniques.

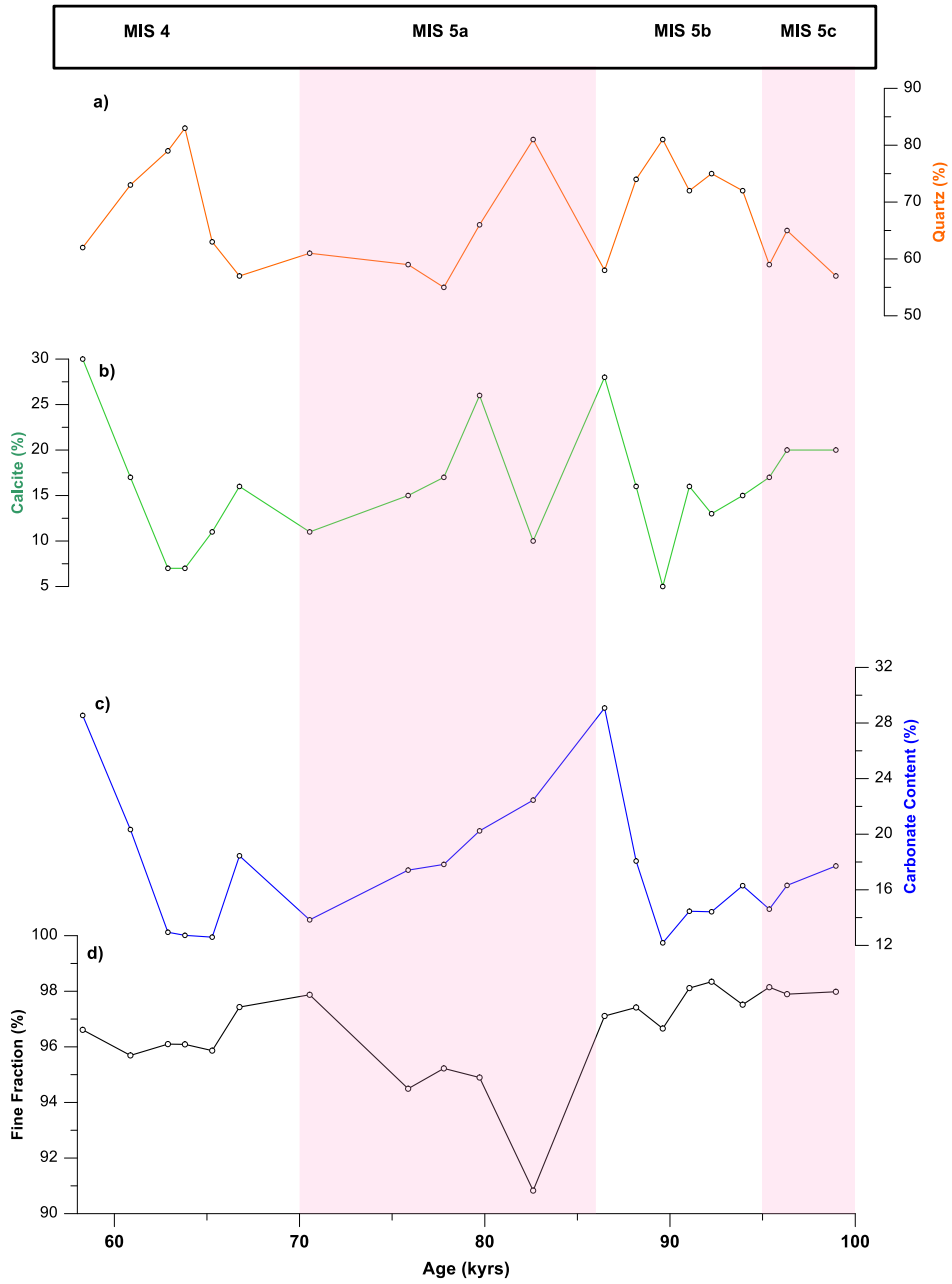

Figure 6. Comparison between the mineralogical and sedimentary data. (**a**) Quartz semi-quantitative content (%). (**b**) Calcite semi-quantitative content (%). (**c**) Carbonate content in the Fine Fraction (%). (**d**) Fine Fraction content (%) compared to the bulk sample.

4. Discussion

4.1. XRF Validation

Accordingly, the curves established with the ICP-OES and XRF are parallels revealing that both measurements presented similar distributions downcore with the same amplitude of values (Figure 3).

On the other hand, the numeric values of the elemental ratios were different when both methods were compared. The XRF measurements always presented higher values than ICP-OES measurements (Table 1), due to a lack of calibration with standard materials in the XRF. Attempting to correct the XRF intensity using the ICP-OES data as a sample with known elementary ratios, a linear regression model was calculated (Figure 4). Both r^2 values calculated were considerate high, 0.875 for lnTi/Ca and 0.755 for lnFe/Ca. Based on the linear equation generated (Figure 4a,b), the logarithmic values of the elementary

XRF ratios were corrected, considerably decreasing the error in the initially generated concentrations, presenting similar curves between the results using the XRF and the ICP-OES techniques (Figure 4c,d).

In both cases, the *t*-test calculated after the calibration revealed that the techniques were in agreement, as the *p*-value was greater than 0.05 for both lnTi/Ca ($p = 0.983$) and lnFe/Ca ($p = 0.869$), demonstrating that the mean of the differences is statistically zero, agreeing that the techniques show similar mean values. This also can be concluded by observing the B-A plot, with only one sample being out of the Lines of Agreement, concluding that the techniques present the same results and the technique with this equipment can be applied.

A high correlation between XRF and ICP-OES for both ln (Ti/Ca) and ln (Fe/Ca) was shown. Such results enabled a linear regression to correct the slightly higher values obtained by XRF. With this correction, both techniques showed very similar results, demonstrating that the BTX-II equipment can perform these analyses with high reliability.

4.2. Paleoceanographic Application

In seawater, Fe and Ti are trace elements, with Ti being highly conservative due to the almost absent use in biological process; in contrast, Fe is a very important micronutrient that can limit primary productivity [27]. In the sediments, these elements have a similar behavior being present mostly in the form of amorphous or poorly crystalline (hydro)oxides (TiO_2 and Fe_2O_3). Moreover, Fe is a major component of many clay minerals derived from soils [28], while Ti weathering rate is very slow and it is considered immobile [29] also if some studies considered it is mobile in soils [30]. Once these elements and minerals are buried, they can suffer reduction or authigenic mobilization/precipitation [31,32]. However, this is more common in organic-rich deposits. For sediments in which terrigenous materials are dominant, the authigenic components are negligible if compared with their fairly high contents in terrestrial detritus [31]. Ca is a major element essential to many organisms in the seawater, since several organisms use it to build their skeletons. Therefore, its content in the sediments reflects directly the biogenic part of the sediment, being represented in the sediments primarily as Calcium Carbonate Content ($CaCO_3$) in the form of calcite or aragonite.

Fe and Ti are elements mainly associated with the terrigenous fraction of the sediment, related to the siliciclastic components of the sediment [1]; in turn, Ca is primarily a component of the marine fraction of the sediment, associated mainly with variations in the carbonate content. Therefore, both of these elemental ratios reflect the relation between the terrigenous input and the marine contribution, and by conclusion do not allow many reliable reconstructions of terrestrial climate conditions, in particular for past climate changes [7].

According to this, the variations of the lnTi/Ca and lnFe/Ca in our record are associated with the oscillation between the marine and terrigenous fraction deposited, with the major terrigenous contributions being observed during the MIS 5b and the MIS 4 (Figure 3). However, elementary ratios using Ca must be looked at carefully, because the dilution and dissolution effects can affect directly Ca concentrations [1,7,19].

Mainly three processes can influence the calcite, as well as Ca, content: the primary production, the dissolution and the dilution made by other types of materials. In the core area, dissolution does not influence the micropaleontological records and the paleoproductivity maxima occur in the same periods of higher terrigenous supply [18]. This leads to the conclusion that the calcite content is controlled mainly by the dilution of the marine fraction by terrigenous input, which can be observed by the mirror distributions in the calcite and quartz content (Figure 6). Therefore, the lnFe/Ca and lnTi/Ca are reliable indicators of the terrigenous sediment input and continental runoff in our study.

When comparing calcite mineral trends with the $CaCO_3$, we observe a similar trend (Figure 6), indicating that calcite is the predominant carbonate phase. Therefore, at least the major component of calcite is presumably from a marine biological source, indicating

that the pelagic deposition is a great contribution process to the bulk sediment in this area. In turn, the Fine Fraction content (FF), which is the percent of sediments with size lesser than 63 μm, does not seem correlated to any of these minerals, revealing that the variations of the minerals are not only due to different grain sizes, but are probably due to changes in the bottom hydrodynamics and mobilization of relict materials.

Some studies already used the variations of minerals (quartz and calcite) as proxies of the oscillations between terrigenous and marine inputs [11,12]. So, in addition to the lnTi/Ca and lnFe/Ca ratios, the content of quartz is also used as an indication of terrigenous materials from the mineralogical perspective. So as expected, the distributions of quartz and lnTi/Ca have a similar pattern (Figure 7), showing higher values during the cold periods, and the inverse for warm periods, demonstrating that the terrigenous input is certainly changing with processes that are in orbital scale, such as precipitation and sea-level changes.

When comparing the results from the mineralogical and elementary components of the sediment with the data from SE Brazil precipitation [33] and global sea-level changes [34], it is clear that both of these processes influence the terrigenous input (Figure 7).

The higher terrigenous supply periods happen at the same time that precipitation rates are higher and the sea-level drops, as we can observe in the MIS 4 and MIS 5b (Figure 7), and the opposite trend is observed at the warmer periods, such as MIS 5a and MIS 5c, where all the terrigenous input proxies show lower values. Costa et al. [18] also identified that precipitation rates strongly control the terrigenous input in SE Brazil.

During the period studied, the South America Monsoon System (SASM) associated with changes in the Intertropical Convergence Zone presented high variability of precipitation patterns [33]. This changes the vegetation of the continent, especially in the colder periods, probably in the same way observed by Behling et al. [19] in the last glacial age, with grassland dominating the landscape reconstructed from terrestrial records. However, Leite et al. [35] found more fragmentation of the Atlantic Forest during interglacial maxima than in the Glacial maxima, detecting expansion of the Atlantic Forest of southeastern Brazil to the exposed shelf during a low stand of sea level.

The higher values of lnTi/Ca, as well as all of the terrigenous input proxies, during the high insolation and precipitation periods [33] indicate that they are also products of periods of more intense weathering and increased river runoff as suggested by other studies [36].

We also applied the Global sea level stack [34] to roughly estimate the variation in this process and compare the diverse terrigenous supply proxies, represented by both minerals and elementary ratios (Figure 7). The global stack suggests low stands of the sea level during the cold stages, MIS 5b and MIS 4, which are the same periods with higher terrigenous supply, indicating that the lower sea level, would also contribute to this higher weathering observed in the precipitation variation.

The lower sea level would leave a greater area of the continental shelf exposed to erosion and the rivers would have drained closer to the upper continental slope. Increased land erosion due to a change in glacial vegetation cover during glacial periods [19,35], caused by changes in precipitation, would also enhance the weathering in the continent leading to a higher terrigenous sediment input. This indicates that continental and marine realms are strongly correlated in this region, which was also observed in Gu et al. [37] who detected changes in the pollen/spore and dinocyst assemblages occurring at similar pacing.

Therefore, the main processes that control the deposition of terrigenous sediments in this area are precipitation and changes in the sea level. Precipitation acts mainly via riverine input, probably due to the higher discharge of Paraíba do Sul or Doce River during these high precipitation periods, such as during MIS5b. The changes in the sea level are related to the exposition of the continental shelf. During the low stands, this area becomes exposed leaving the sediments more susceptible to erosion, and at the same time, the sediments in the source area have an easier path to the core area.

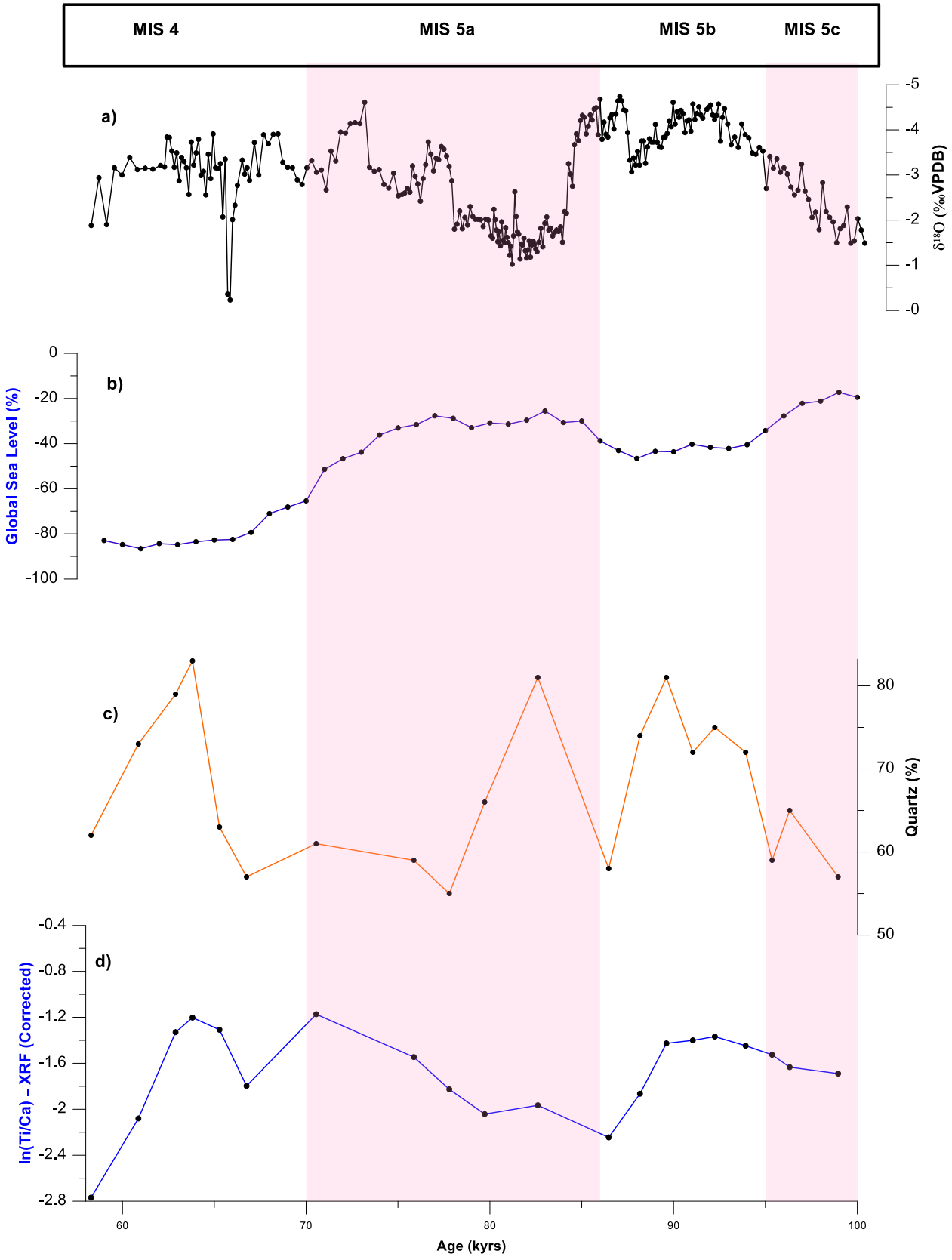

Figure 7. Terrigenous supply proxies compared to precipitation and sea level. (**a**) Oxygen isotopes ratio ($\delta^{18}O$) in stalagmite BT2 [33] in the Botuverá cave, showing the precipitation pattern in the southeast Brazil, with the lower values in the warmer periods, MIS 5a and 5c. (**b**) Global sea level stack [34]. (**c**) Quartz semi-quantitative measures. (**d**) ln(Ti/Ca) along the period studied.

5. Conclusions

The mineralogical and elementary results of XRF measurements (BTX II) presented here were compared to destructive methods (ICP-OES) and confirm the viability of such a technique, although further studies are needed to confirm this for different rock classes.

With this new calibration of the equipment, using a very low quantity of material, we were able to construct a stratigraphic sequence of minerals and elements associations with a cheap, fast, non-destructible technique that can be applied in high-resolution records.

By comparing the mineralogical and elementary data, we were able to conclude that the terrigenous input is higher during the colder periods and lower in the warmer periods, with the sea-level changes and precipitation being the main influencers controlling the variations of terrigenous supply to the Brazilian Continental Margin.

Author Contributions: G.A.P.: writing—original draft. K.B.C.: conceptualization, review, editing. F.A.L.T.: project administration, resources, review. M.O.T.: formal analysis, investigation, review, editing. L.J.: project administration, software, review, conceptualization, writing. All authors have read and agreed to the published version of the manuscript.

Funding: This research was funded by São Paulo Research Foundation (FAPESP) grant 16/24946-9.

Institutional Review Board Statement: Not applicable.

Informed Consent Statement: Not applicable.

Data Availability Statement: The data newly presented in this study are openly available in FigShare at [https://doi.org/10.6084/m9.figshare.14884755.v1] (accessed on 18 May 2021).

Acknowledgments: This study was funded by the São Paulo Research Foundation (FAPESP) grant 16/24946-9. The authors wish to express their thanks to Petrobras for providing the samples for our study. Acknowledgements are also due to the anonymous reviewers for their insightful suggestions.

Conflicts of Interest: The authors declare no conflict of interest. The funders had no role in the design of the study; in the collection, analyses, or interpretation of data; in the writing of the manuscript, or in the decision to publish the results.

References

1. Arz, H.W.; Pätzold, J.; Wefer, G. Correlated millennial-scale changes in surface hydrography and terrigenous sediment yield inferred from last-glacial marine deposits off Brazil. *Quat. Res.* **1998**, *50*, 157–166. [CrossRef]
2. Mahiques, M.M.; Tessler, M.G.; Ciotti, A.M.; Da Silveira, I.C.A.; e Sousa, S.H.D.M.; Figueira, R.C.L.; Tassinari, C.C.G.; Furtado, V.V.; Passos, R.F. Hydrodynamically driven patterns of recent sedimentation in the shelf and upper slope off Southeast Brazil. *Cont. Shelf Res.* **2004**, *24*, 1685–1697. [CrossRef]
3. Luz, L.G.; Santos, T.P.; Eglinton, T.I.; Montluçon, D.; Ausin, B.; Haghipour, N.; Sousa, S.M.; Nagai, R.H.; Carreira, R.S. Contrasting late-glacial paleoceanographic evolution between the upper and lower continental slope of the western South Atlantic. *Clim. Past* **2020**, *16*, 1245–1261. [CrossRef]
4. Araujo, L.D.; Lobo, F.J.; De Mahiques, M.M. The imprint of sedimentary processes in the acoustic structure of deposits on a current-dominated continental shelf. *J. S. Am. Earth Sci.* **2021**, *105*, 103005. [CrossRef]
5. Behling, H.; Arz, H.W.; Pätzold, J.; Wefer, G. Late Quaternary vegetational and climate dynamics in northeastern Brazil: Inferences from marine core GEOB 3104-1. *Quat. Sci. Rev.* **2000**, *19*, 981–994. [CrossRef]
6. Röhl, U.; Bralower, T.J.; Norris, R.D.; Wefer, G. New chronology for the late Paleocene thermal maximum and its environmental implications. *Geology* **2000**, *28*, 927–930. [CrossRef]
7. Govin, A.; Holzwarth, U.; Heslop, D.; Keeling, L.F.; Zabel, M.; Mulitza, S.; Collings, J.A.; Chiessi, C.M. Distribution of major elements in Atlantic surface sediments (36° N–49° S): Imprint of terrigenous input and continental weathering. *Geochem. Geophys. Geosyst.* **2012**, *13*, 1–23.
8. Weltje, G.J.; Tjallingii, R. Calibration of XRF core scanners for quantitative geochemical logging of sediment. *Earth Planet. Sci. Lett.* **2008**, *274*, 423–438. [CrossRef]
9. Rothwell, R.G.; Rack, F.R. *New Techniques in Sediment Core Analysis: An Introduction*; Special Publication; Geological Society: London, UK, 2006; Volume 267, pp. 1–29.
10. Boss, C.B.; Fredeen, K.J. *Concepts, Instrumentation, and Techniques in Inductively Coupled Plasma Optical Emission Spectrometry*; Perkin Elmer Corporation: Shelton, CT, USA, 1997.
11. Stein, R.; Hefter, J.; Grützner, J.; Voelker, A.; Naafs, B.D.A. Variability of surface water characteristics and Heinrich-like events in the Pleistocene midlatitude North Atlantic Ocean: Biomarker and XRD records from IODP Site U1313 (MIS 16–9). *Paleoceanography* **2009**, *24*. [CrossRef]

12. Li, J.; Liu, S.; Shi, X.; Zhang, H.; Fang, X.; Cao, P.; Yang, C.; Xue, X.; Khokiattiwong, S.; Kornkanitnan, N. Sedimentary responses to the sea level and Indian summer monsoon changes in the central Bay of Bengal since 40 ka. *Marine Geol.* **2019**, *415*, 105947. [CrossRef]
13. Savian, J.F.; Jovane, L.; Frontalini, F.; Trindade, R.I.; Coccioni, R.; Bohaty, S.M.; Wilson, P.A.; Florindo, F.; Roberts, A.P.; Catanzariti, R.; et al. Enhanced primary productivity and magnetotactic bacterial production in response to middle Eocene warming in the Neo-Tethys Ocean. *Palaeogeogr. Palaeoclimatol. Palaeoecol.* **2014**, *414*, 32–45. [CrossRef]
14. Savian, J.F.; Jovane, L.; Giorgioni, M.; Iacoviello, F.; Rodelli, D.; Roberts, A.P.; Chang, L.; Florindo, F.; Sprovieri, M. Environmental magnetic implications of magnetofossil occurrence during the Middle Eocene Climatic Optimum (MECO) in pelagic sediments from the equatorial Indian Ocean. *Palaeogeogr. Palaeoclimatol. Palaeoecol.* **2016**, *441*, 212–222. [CrossRef]
15. Cornaggia, F.; Jovane, L.; Alessandretti, L.; Alves De Lima Ferreira, P.; Lopes Figueira, R.C.; Rodelli, D.; Berbel, G.B.B.; Braga, E.S. Diversions of the Ribeira River Flow and Their Influence on Sediment Supply in the Cananeia-Iguape Estuarine-Lagoonal System (SE Brazil). *Front. Earth Sci.* **2016**, *6*, 25. [CrossRef]
16. Sarrazin, P.; Blake, D.; Feldman, S.; Chipera, S.; Vaniman, D.; Bish, D. Field Deployment of a Portable XRD/XRF Instrument on Mars Analog Terrain. *Adv. X-ray Anal.* **2005**, *48*, 194–203.
17. Blake, D.; Vaniman, D.; Achilles, C.; Anderson, R.; Bish, D.; Bristow, T.; Chen, C.; Chipera, S.; Crisp, J.; Des Marais, D.; et al. Characterization and calibration of the CheMin mineralogical instrument on Mars Science Laboratory. *Space Sci. Rev.* **2012**, *170*, 341–399. [CrossRef]
18. Costa, K.B.; Cabarcos, E.; Santarosa, A.C.A.; Battaglin, B.B.F.; Toledo, F.A.L. A multiproxy approach to the climate and marine productivity variations along MIS 5 in SE Brazil: A comparison between major components of calcareous nannofossil assemblages and geochemical records. *Palaeogeogr. Palaeoclimatol. Palaeoecol.* **2016**, *449*, 275–288. [CrossRef]
19. Behling, H.; Arz, H.W.; Pätzold, J.; Wefer, G. Late Quaternary vegetational and climate dynamics in southwestern Brazil: Inferences from marine cores GEOB 3229-2 and GeoB 3202-1. *Palaeogeogr. Palaeoclimatol. Palaeoecol.* **2002**, *179*, 227–243. [CrossRef]
20. Schlitzer, R. Ocean Data View, v.4.7.10. 2017. Available online: https://odv.awi.de/ (accessed on 30 June 2021).
21. Wang, X.; Auler, A.S.; Edwards, R.L.; Cheng, H.; Cristalli, P.S.; Smart, P.L.; Richards, D.A.; Shen, C.C. Wet periods in northeastern Brazil over the past 210 kyr linked to distant climate anomalies. *Nature* **2004**, *432*, 740–743. [CrossRef]
22. Degen, T.; Sadki, M.; Bron, E.; König, U.; Nénert, G. The highscore suite. *Powder Diffr.* **2014**, *29*, S13–S18. [CrossRef]
23. Bland, J.M.; Altman, D.G. Applying the right statistics: Analyses of measurement studies. *Ultrasound Obstet. Gynecol.* **2003**, *22*, 85–93. [CrossRef]
24. Melkonyan, G.A. A statistical comparison between the performance of ICP-OES and XRF methods for the analysis of trace amount of hg in urban soil samples. *Electron. J. Nat. Sci.* **2020**, *34*, 51–56.
25. Balestra, B.; Rose, T.; Fehrenbacher, J.; Knobelspiesse, K.D.; Huber, B.T.; Gooding, T.; Paytan, A. In Situ Mg/Ca Measurements on Foraminifera: Comparison Between Laser Ablation Inductively Coupled Plasma Mass Spectrometry and Wavelength-Dispersive X-Ray Spectroscopy by Electron Probe Microanalyzer. *Geochem. Geophys. Geosyst.* **2021**, *22*. [CrossRef]
26. Hammer, Ø.; Harper, D.A.; Ryan, P.D. PAST: Paleontological statistics software package for education and data analysis. *Palaeontol. Electron.* **2001**, *4*, 9.
27. Geider, R.J.; La Roche, J. The role of iron in phytoplankton photosynthesis, and the potential for iron-limitation of primary productivity in the sea. *Photosynth. Res.* **1994**, *39*, 275–301. [CrossRef]
28. Taylor, K.G.; Macquaker, J.H.S. Iron Minerals in Marine Sediments Record Chemical Environments. *Elements* **2011**, *7*, 113–118. [CrossRef]
29. Hutton, J.T. *Minerals in Soil Environment*; Dixon, J.B., Weed, S.B., Eds.; Soil Science Society of America: Madison, WI, USA, 1977.
30. Correns, C.W.; Wedepohl, K.H. (Eds.) *Handbook of Geochemistry*; Springer: Berlin, Germany, 1969; Volume 2.
31. Wei, G.; Liu, Y.; Li, X.; Shao, L.; Liang, X. Climatic impact on Al, K, Sc and Ti in marine sediments: Evidence from ODP Site 1144, South China Sea. *Geochem. J.* **2003**, *37*, 593–602. [CrossRef]
32. Sun, G.; Wang, Y.; Guo, J.; Wang, M.; Jiang, Y.; Pan, S. Clay Minerals and Element Geochemistry of Clastic Reservoirs in the Xiaganchaigou Formation of the Lenghuqi Area, Northern Qaidam Basin, China. *Minerals* **2019**, *9*, 678. [CrossRef]
33. Cruz, F.W., Jr.; Burns, S.J.; Karmann, I.; Sharp, W.D.; Vuille, M.; Cardoso, A.O.; Ferrari, J.A.; Silva-Dias, P.L.; Viana, O., Jr. Insolation-driven changes in atmospheric circulation over the past 116,000 years in subtropical Brazil. *Nature* **2005**, *434*, 63–66. [CrossRef]
34. Spratt, R.M.; Lisiecki, L.E. A Late Pleistocene sea level stack. *Clim. Past* **2016**, *12*, 1079–1092. [CrossRef]
35. Leite, Y.L.; Costa, L.P.; Loss, A.C.; Rocha, R.G.; Batalha-Filho, H.; Bastos, A.C.; Quaresma, V.S.; Fagundes, V.; Passamani, M.; Pardini, R. Neotropical forest expansion during the last glacial period challenges refuge hypothesis. *Proc. Natl. Acad. Sci. USA* **2016**, *113*, 1008–1013. [CrossRef]
36. Nace, T.E.; Baker, P.A.; Dwyer, G.S.; Silva, C.G.; Rigsby, C.A.; Burns, S.J.; Giosan, L.; Otto-Bliesner, B.; Liu, Z.; Zhu, J. The role of North Brazil Current transport in the paleoclimate of the Brazilian Nordeste margin and paleoceanography of the western tropical Atlantic during the late Quaternary. *Palaeogeogr. Palaeoclimatol. Palaeoecol.* **2014**, *415*, 3–13. [CrossRef]
37. Gu, F.; Zonneveld, K.A.; Chiessi, C.M.; Arz, H.W.; Pätzold, J.; Behling, H. Long-term vegetation, climate and ocean dynamics inferred from a 73,500 years old marine sediment core (GeoB2107-3) off southern Brazil. *Quat. Sci. Rev.* **2017**, *172*, 55–71. [CrossRef]